Field dependence of micromagnetic domain patterns in MnAs films

R. Engel-Herbert, T. Hesjedal,[a] J. Mohanty, D. M. Schaadt, and K. H. Ploog
Paul-Drude-Institut für Festkörperelektronik, Hausvogteiplatz 5-7, D-10117 Berlin, Germany

(Received 30 June 2005; accepted 16 August 2005; published online 30 September 2005)

We have studied the domain behavior of submicrometer wide ferromagnetic stripes by magnetic force microscopy (MFM) in the presence of an *in situ* magnetic field. MFM images in the demagnetized state show alternatingly magnetized domains fully extended across the stripe. Moreover, domain structures are found to exhibit a substructure across the stripe. Increasing fields drive out the domain walls of the complex domains first, leaving the alternating domains behind. The remaining magnetization process aligns increasing parts of the domains along the field direction by gradually shrinking the width of oppositely magnetized domains rather than by flipping larger areas at once. Micromagnetic simulations confirm the observed behavior. The simulations reveal that flipping of the domains occurs only when a magnetic pinning center is involved. © *2005 American Institute of Physics*. [DOI: 10.1063/1.2060959]

I. INTRODUCTION

Ferromagnetic MnAs is a promising candidate for electrical spin injection into GaAs- and Si-based semiconductor structures,[1] since it exhibits a Curie temperature of 40 °C, a comparably high saturation magnetization, and a relatively small coercive field of 50 Oe. Although there is the difference in crystal symmetry of hexagonal α-MnAs and cubic GaAs and a large anisotropic lattice mismatch of up to 30%, MnAs films of high structural perfection can be epitaxially grown on GaAs (001), (110), (111), and (311),[2–5] as well as on Si (001) and (111).[6] As a result of the epitaxial constraints of MnAs/GaAs(001) heterostructures, where the in-plane lattice spacings a and c cannot change during the first-order phase transition, the ferromagnetic α and the nonferromagnetic β phase coexist over a wide temperature range of 10–40 °C. The two phases arrange themselves in a unique periodic stripe pattern oriented along the MnAs[0001] (c axis) direction thereby reducing the strain.[7–9] The understanding of magnetic phenomena in these sub-micron scale structures is essential to applications of these materials in magnetoelectronics. Here, we study the domain structure of the coupled ferromagnetic stripe structure in an *in situ* magnetic field by magnetic force microscopy (MFM) and by micromagnetic simulations.

II. EXPERIMENTS

A commercial MFM (Ref. 10) was equipped with a variable magnetic-field setup.[11] Silicon nitride cantilevers with a spring constant of 0.05 N/m, sputter coated with 60 nm Co/Cr were used as magnetic probes.[12] The tips have an effective radius of roughly 80 nm. The cantilevers were magnetized along their tip axis to saturation.

We have investigated a 180-nm-thick MnAs film on GaAs(001) that was grown in the so-called A orientation with the following epitaxial relationship: MnAs($\bar{1}100$) ‖GaAs(001) and MnAs[0001](c axis)‖GaAs[$1\bar{1}0$]. MnAs exhibits an uniaxial magnetocrystalline anisotropy with the c axis being the hard axis of magnetization.[13] The shape anisotropy of the film prefers the in-plane a-axis direction (MnAs[$11\bar{2}0$]), which exhibits an easy axis behavior.[14]

In the demagnetized state, MnAs films on GaAs(001) exhibit different types of domains, where the magnetic moments are aligned along the a-axis direction.[16] In recent temperature-dependent MFM studies we observed that each individual ferromagnetic stripe can break up along the easy axis direction into up to three subdomains with opposite magnetization directions, termed type (I)–(III).[15,16] The demagnetized state was prepared by heating the film above the phase-transition temperature until it is completely in its β phase and then cooling it down to room temperature in zero field. A typical MFM micrograph [Fig. 1(a)] shows predominantly type (I) domains where the stripe is single domain across its width. The position of the ferromagnetic (FM) and

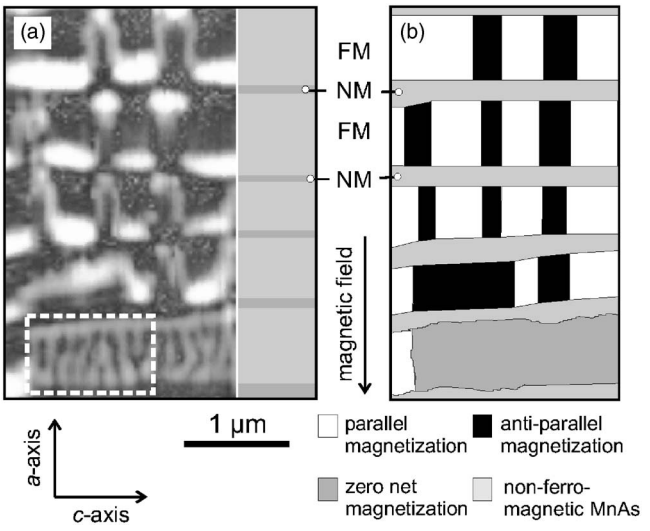

FIG. 1. (a) MFM image of the MnAs film in the demagnetized state. The ferromagnetic and nonferromagnetic stripes are indicated on the right-hand side of the figure. (b) Corresponding magnetization distribution showing areas of parallel, antiparallel, and zero net magnetization. Nonferromagnetic β-phase areas show light grey contrast.

[a]Electronic mail: hesjedal@pdi-berlin.de

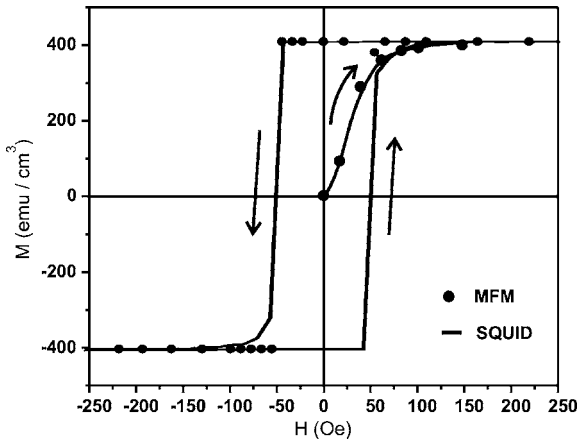

FIG. 2. Hysteresis curve measured at room temperature with the field applied along the easy axis of magnetization (*a* axis). The solid line shows the SQUID measurement and the black circles indicate the values obtained by field-dependent MFM. The value for the coercive field is ±50 Oe.

nonferromagnetic stripes (NM) are sketched on the right-hand side. Domains of alternating orientation in combination with 180° Bloch walls were assumed to lead to the observed meander-shaped pattern.[14] The out-of-plane components of the stray field at the ends of the domains, as well as the 180° Bloch walls pointing into and out of the film plane along the domain boundaries are mapped by MFM. Moreover, more complex domain structures are regularly observed (see dashed rectangle) that are explained with the help of contrast simulations by a combination of type (I) and (III) domains.[16]

Field-dependent MFM is a method for obtaining the magnetization of a magnetic sample on a microscopic scale. In case of MnAs with its in-plane easy and hard axes, the relative magnetization is obtained by simply registering the parallel and antiparallel magnetized domains of the ferromagnetic stripes as a function of the applied field. The analysis of the presented MFM image is shown in Fig. 1(b), where the domains oriented parallel to the applied magnetic field are marked white and the antiparallel-oriented domains black. Previous simulations have shown that the more complex domain patterns, such as the one highlighted by the dashed rectangle in (a), have a vanishing net magnetization [marked white in (b)].[17] Absolute values for the magnetization are obtained by multiplying the deduced relative values with the magnetization of the fully magnetized state measured by superconductive quantum interference device (SQUID) at 1.5 kOe. The values are shown as black circles in Fig. 2.

Moreover, Fig. 2 shows the hysteresis curve along with the virgin curve measured by SQUID magnetometry at room temperature (solid line). The field was applied along the in-plane *a*-axis direction. Prior to the measurement of the virgin curve, the sample was demagnetized in an alternating magnetic field. The ratio of the remanent magnetization to the saturation magnetization M_r/M_s is close to unity. This indicates that the reversible part of the magnetization is very small, as expected for coupled ferromagnetic stripes. The coercive field obtained by both methods yields ±50 Oe.

Figure 3 shows selected room-temperature MFM images as a function of applied magnetic field for the virgin magnetization curve of the same sample area. Representative sample spots, showing type (I), (II), and a complex (III)-related domain, are highlighted by a white circle and rectangles, respectively. The type (III)-related domain was explained by a sequence of type (I) and (III) domains.[16] A schematic of the magnetization distribution for an alternating type (I) domain is illustrated by the arrows in the black box. Starting from a field value between 10 and 20 Oe, the type (III)-related domains start to transform into type (I) domains. The last type (III)-related domains are driven out between 40 and 60 Oe. Type (II) domains, on the other hand, transform into type (I) domains between 20 and 40 Oe. Upon a further increase of the field, the remaining type (I) domains get oriented in the field direction until, above 100 Oe, all ferromagnetic stripes are in a single domain state (cf. black box). Interestingly, the few type (I) domains that remain antiparallely magnetized up to above 100 Oe are correlated across the stripes (cf. middle of Fig. 3). At lower fields, these domains further exhibit irregular domain walls, different from the other antiparallely magnetized sections of the film that flip at lower fields.

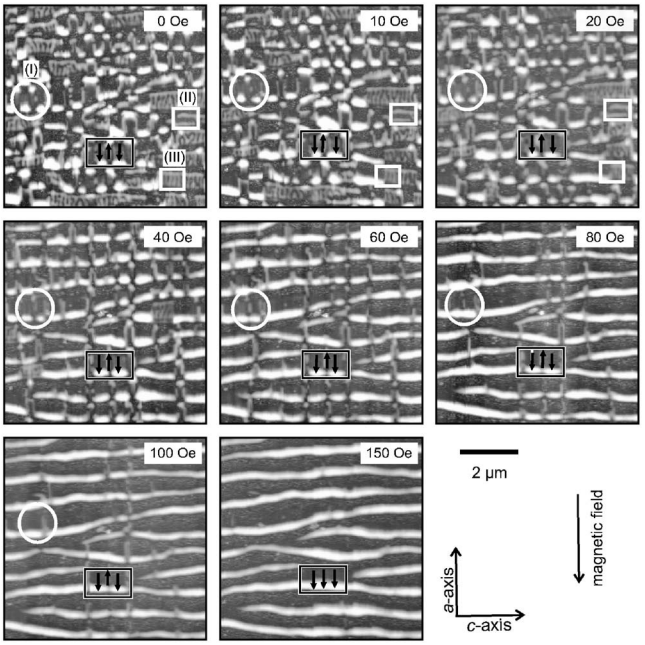

FIG. 3. Room-temperature field-dependent MFM measurements on a 180-nm-thick MnAs film on GaAs(001): The sequence shows selected MFM scans recorded along the virgin curve. The field of 0–200 Oe was applied along the easy axis direction, as indicated. The development of the three basic domain types can be followed looking at the white circular and rectangular markers. The domain configuration of a particular area with type (I) domains is highlighted (see black box).

III. MICROMAGNETIC SIMULATIONS

In order to get a deeper insight into the intrastripe domain structure and interstripe coupling, we performed micromagnetic simulations. Since MnAs films exhibit an easy plane of magnetization perpendicular to the *c* axis that plays an increasing role with decreasing contribution of the shape anisotropy for thicker films, a three-dimensional micromagnetic simulation code has to be employed.[17] The modeled 182-nm-thick sample piece consists of two ferromagnetic

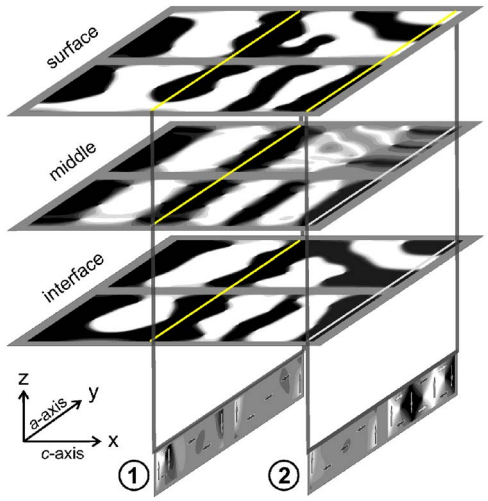

FIG. 4. Magnetization distribution of the relaxed state at zero applied field. The in-plane magnetization distribution M_y is visualized at three positions in film depth (z=const), at the surface, in the middle of the film, and at the interface with the substrate. The cross-sectional cuts along the a axis (x =const) show the z component of the magnetization M_z at the positions labeled ① and ②.

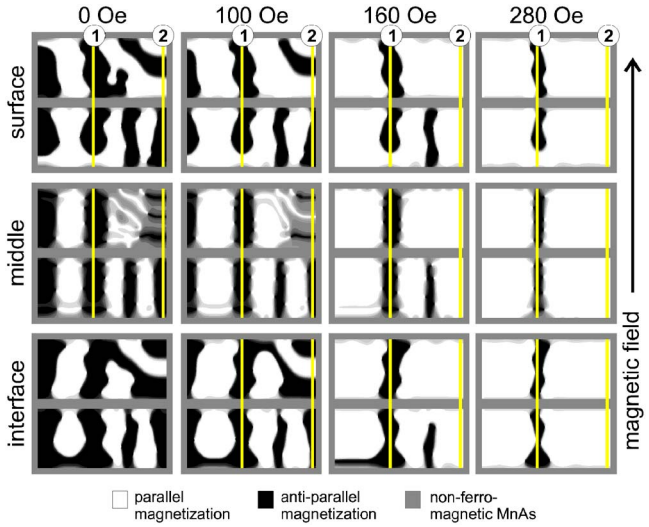

FIG. 5. Field dependence of the in-plane magnetization distribution M_y at the surface, in the middle, and at the interface of the film with GaAs. The direction of the applied magnetic field is shown on the right-hand side. The lines ① and ② indicate the positions of the cross sections shown in Fig. 6.

stripes of a width of 732 nm, separated by a 200-nm-wide nonferromagnetic stripe. This corresponds to an α-phase fraction of 0.88, which is observed for 180-nm-thick films at 21 °C. The sample was divided into $128\times128\times14$ cells (length × width × thickness) of $(13\ \text{nm})^3$. In order to ensure a good numerical conversion, the appropriate cell dimensions have to be chosen to be of the order of the micromagnetic exchange length (5 nm in the case of MnAs). The simulation of smaller test structures have shown that a cell size of $(13\ \text{nm})^3$ is a good compromise between physical demands and calculation time. The following parameters for MnAs were used in the simulation: exchange stiffness constant $A=1.0\times10^{-11}$ J/m, saturation magnetization $M_s=4\times10^5$ A/m, and magnetocrystalline anisotropy constants $K_{u1}=-7.2\times10^5$ J/m^3 and $K_{u2}=-3.6\times10^5$ J/m^3. The x axis of the coordinate system of the simulator corresponds to the magnetocrystalline hard axis (c axis), the y-z plane to the easy plane, and the z axis is along the film normal.

As a start configuration, the ferromagnetic α stripes were assumed to be demagnetized. The random magnetization was allowed to relax at zero applied field, the result is shown in Fig. 4. The in-plane component of the magnetization is shown for z=const at the surface (above), in the middle of the film (middle), and at the interface with GaAs (below). The distribution of the z component of the magnetization in depth of selected cross-sectional cuts labeled ① and ② is shown below. Note that the x component of the magnetization is not shown. The strong uniaxiality of the system prevents the magnetization in x direction, as the magnitude is always smaller than 1/50 of the total magnetization.

Three main domain types are identified, consistent with the MFM findings: Type (I) is characterized by a uniform magnetization along the a axis, also largely uniform in depth. However, the simple picture of a bar-magnet-like behavior has to be corrected due to the formation of closure-type domains at the edges of the stripe (see cross-sectional cuts for details). Type (II) domains originate from oppositely magnetized areas, as can be seen in cross section ① below. The simulations show that the surface magnetization distribution that led to the classification scheme does not reach through the film. In fact, a single "diamond" state turns out to be the origin of the type (II) stray fields. A type (III) domain is found along line ② above. The initial threefold separation of the magnetization on the surface splits further up towards the middle of the film and becomes threefold again close to the interface (inverted magnetization). The cross section ② (above) reveals that the type (III) domains commonly observed in MFM are due to a double diamond state.

Next, we studied the stability of the simulated domain structure in an applied magnetic field. The field was applied in the $+x$ direction, increasing in steps of 25 up to 100 Oe and in steps of 60 Oe beyond. The magnetization distributions, for selected field values of 0, 100, 160, and 280 Oe are shown in Figs. 5 (M_y) and 6 (M_z). Upon applying a magnetic field of 100 Oe, a domain wall movement is obvious that leads to an increase of parallel magnetized domains and a reduction of the overall domain wall length. A flipping of the domains occurs from 160 Oe on, however, smaller antiparallely magnetized sections remain. Their existence is due to a pinning by a vortexlike domain configuration. The vortexlike features are visible as distortions of the straight domain walls, e.g., in Fig. 4, middle, and are persistent up to the disappearance of the antiparallely magnetized domains. The cross-sectional images (Fig. 6) reveal the vortexlike state on the left-hand side of trace ①. At 280 Oe, the antiparallely oriented domains shrink further and disappear above 320 Oe. In MFM, the distortions of the domain walls are difficult to resolve, however, the experiments also reveal that the domains that flip at the highest applied field exhibit an irregular domain wall structure at lower fields. Note the difference between the diamond state and the vortexlike state (Fig. 6, trace ① left-hand side versus Fig. 6, trace ② right-hand side). Whereas the diamond state shows a rotation of the diamond

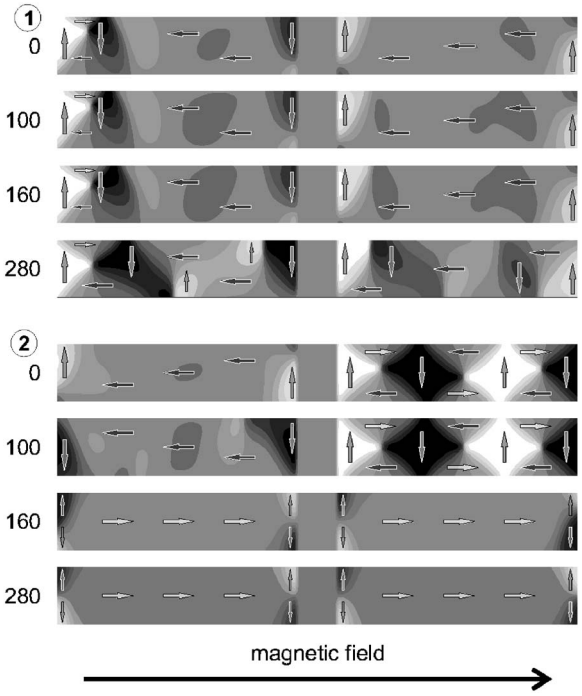

FIG. 6. Field dependence of the the out-of-plane magnetization distribution of two selected cuts, indicated by lines ① and ② in Fig. 5.

with increasing field, thereby reducing the antiparallely oriented moments, the vortexlike state remains pinned.

In order to correlate the simulated domain structure with the experimental observations, we calculated the stray field at a distance of 100 nm above the surface (Fig. 7), i.e., at a typical distance for MFM measurements. The stray field at a certain height is calculated by the summation of the in-plane and out-of-plane magnetic field contributions obtained from the dipole approximation of the magnetization distribution. The measurement plane is sampled by a 50×50 points grid with a step size of $\Delta x = \Delta y = 40$ nm. In general, the simulated stray field images reproduce well the typically measured MFM contrast. At zero applied field, type (I), (II), and (III) domains are observed. With increasing field, type (II) and (III) domains vanish. A small number of domains remain antiparallely magnetized. Their size decreases by domain wall movement. These domains are strongly coupled across the stripes and the domain walls exhibit pinning centers (see Fig. 6 for details). Finally, the pinned domains flip above 280 Oe. This behavior agrees qualitatively well with the MFM observations.

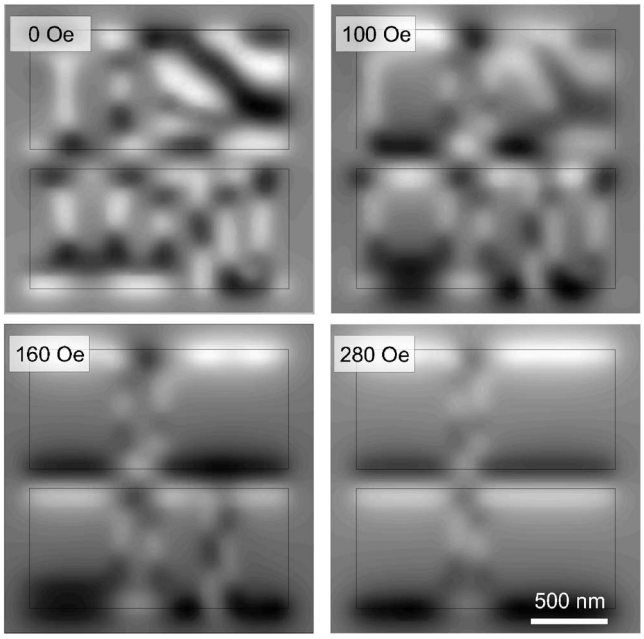

FIG. 7. Calculated stray field (z component) at a height of 100 nm above the sample at the respective applied magnetic-field values. The positions of the ferromagnetic stripes are indicated by rectangles.

IV. CONCLUSIONS

In conclusion, we have studied the field dependence of the micromagnetic domain pattern of coupled ferromagnetic stripes in MnAs films on GaAs(001). Variable-field MFM studies reproduce the magnetic hysteresis curve, as well as the virgin curve, on a microscopic scale. The obtained coercive field value agrees within the experimental uncertainties. Applying a magnetic field on a demagnetized sample reveals the stability of the observed domain types. First, complicated domains transform into simpler domains already at small applied fields. Upon further increasing the field, the magnetization aligned with the field increases continuously by domain wall movement. The remaining antiparallel domains are pinned and finally flip at the highest field values. Three-dimensional micromagnetic simulations reveal that the existence of an easy plane of magnetization causes unexpected in-depth domain structures. This leads, for example, to the observed pinning by a vortexlike magnetization pattern. Furthermore, the higher order domain types commonly observed in MFM experiments can be explained as in-depth domains resulting in complex stray fields.

ACKNOWLEDGMENTS

We thank D. Kolovos-Vellianitis and L. Däweritz for valuable discussions and C. Herrmann for the sample preparation.

[1] M. Ramsteiner *et al.*, Phys. Rev. B **66**, 081304(R) (2002).
[2] M. Tanaka, J. P. Harbison, M. C. Park, Y. S. Park, T. Shin, and G. M. Rothberg, J. Appl. Phys. **76**, 6278 (1994).
[3] M. Tanaka, Physica E (Amsterdam) **2**, 372 (1998).
[4] F. Schippan, A. Trampert, L. Däweritz, and K. H. Ploog, J. Vac. Sci. Technol. B **17**, 1716 (1999).
[5] D. Kolovos-Vellianitis, C. Herrmann, L. Däweritz, and K. H. Ploog, Appl. Phys. Lett. **87**, 092505 (2005).
[6] A. M. Nazmul, H. Shimizu, and M. Tanaka, J. Appl. Phys. **87**, 6791 (2000).
[7] L. Däweritz *et al.*, in *Proceedings of the 28th International Symposium on Compound Semiconductors*, edited by Y. Arakawa, Y. Hirayama, K. Kishino, and H. Yamaguchi, IOP Conf. Proc. Ser. 170, 269–274 (2002).
[8] T. Plake, M. Ramsteiner, V. M. Kaganer, B. Jenichen, M. Kästner, L. Däweritz, and K. H. Ploog, Appl. Phys. Lett. **80**, 2523 (2002).
[9] V. M. Kaganer, B. Jenichen, F. Schippan, W. Braun, L. Däweritz, and K. H. Ploog, Phys. Rev. B **66**, 045305 (2002).
[10] Park Scientific Instruments, M5.
[11] J. Mohanty, R. Engel-Herbert, and T. Hesjedal, Appl. Phys. A: Mater. Sci. Process. **81**, 1359 (2005).
[12] Veeco MSNC-MFMT-A.

[13]R. W. De Blois and D. S. Rodbell, Phys. Rev. **130**, 1347 (1963).
[14]F. Schippan, G. Behme, L. Däweritz, K. H. Ploog, B. Dennis, K.-U. Neumann, and K. R. A. Ziebeck, J. Appl. Phys. **88**, 2766 (2000).
[15]R. Engel-Herbert, J. Mohanty, A. Ney, T. Hesjedal, L. Däweritz, and K. H. Ploog, Appl. Phys. Lett. **84**, 1132 (2004).
[16]T. Plake, T. Hesjedal, J. Mohanty, M. Kästner, L. Däweritz, and K. H. Ploog, Appl. Phys. Lett. **82**, 2308 (2003).
[17]R. Engel-Herbert, T. Hesjedal, and D. Schaadt (unpublished).